UC Santa Barbara
UC Santa Barbara Previously Published Works

Title
Extended defects in epitaxial Sc2O3 films grown on (111) Si

Permalink
https://escholarship.org/uc/item/9tt6n8vm

Journal
Applied Physics Letters, 86

Authors
Klenov, Dmitri O
Edge, Lisa F
Schlom, Darell G
et al.

Publication Date
2005

Peer reviewed

eScholarship.org Powered by the California Digital Library
University of California

Applied Physics Letters ***86****, art.-no. 051901 (2005).*

Extended defects in epitaxial Sc_2O_3 films grown on (111) Si

Dmitri O. Klenov [a)]

Materials Department, University of California, Santa Barbara, CA 93106-5050

Lisa F. Edge and Darrell G. Schlom

Department of Materials Science and Engineering, Pennsylvania State University,

University Park, PA 16802-5005

Susanne Stemmer

Materials Department, University of California, Santa Barbara, CA 93106-5050

[a)] Electronic address: d.o.klenov@physics.org

*Applied Physics Letters **86**, art.-no. 051901 (2005).*

Abstract

Epitaxial Sc_2O_3 films with the cubic bixbyite structure were grown on (111) Si by reactive molecular beam epitaxy. High-resolution transmission electron microscopy (HRTEM) revealed an abrupt, reaction-layer free interface between Sc_2O_3 and Si. The ~ 10% lattice mismatch between Si and Sc_2O_3 was relieved by the formation of a hexagonal misfit dislocation network with Burgers vectors of $1/2\langle\bar{1}10\rangle_{Si}$ and line directions parallel to $\langle 11\bar{2}\rangle_{Si}$. A high density of planar defects and threading dislocations was observed. Analysis of lattice shifts across the planar defects in HRTEM showed that these faults were likely antiphase boundaries (APBs). ABPs form when film islands coalesce during growth because films nucleate with no unique arrangement of the ordered oxygen vacancies in the bixbyite structure relative to the Si lattice.

Further scaling of complementary metal-oxide-silicon field-effect transistors (MOSFETs) is thought to require the use of alternative gate dielectrics with higher dielectric constants [1]. Epitaxial gate dielectrics afford atomically abrupt interfaces with Si that are required for the ultimate scaling of MOSFETs. Epitaxial oxide/Si heterostructures are also of interest as templates for the integration of epitaxial functional materials with Si [2]. Binary insulators with the cubic fluorite structure, and its derivatives, are known to grow epitaxially on (111) oriented Si [3-10]. Oxides with the pyrochlore and bixbyite structures are vacancy-ordered derivatives of the fluorite structure and have lattice parameters that are approximately twice that of Si. A close lattice match with Si and other semiconductors can be achieved by alloying [5,11].

Extended defects, such as planar faults and dislocations, may determine the utility of novel oxide/Si heterostructures for devices because defects may be replicated into active device layers that are subsequently grown on them. Defects, such as misfit dislocations, at the Si/gate dielectric interface influence the mobility of charge carriers in the underlying channel. The goal of this paper is to investigate the nature and origin of extended defects in bixbyite/Si epitaxy by investigating the microstructure of Sc_2O_3 films grown on (111) Si. Sc_2O_3 has the cubic bixbyite structure (space group $Ia\overline{3}$) and its lattice mismatch with Si, defined as $(2a_{\mathrm{Si}} - a_{\mathrm{Sc_2O_3}})/a_{\mathrm{Sc_2O_3}}$, is about 10 % ($a_{\mathrm{Si}} = 0.5431$ nm and $a_{\mathrm{Sc_2O_3}} = 0.9845$ nm [12]). Sc_2O_3 has recently attracted interest as a gate dielectric for Si and GaN-based devices, due to its relatively high dielectric constant (13-14 [13,14]), large reported band gap of ~6 eV [14,15] and predicted thermodynamic stability in contact with Si [16].

35 nm thick Sc_2O_3 films were grown on 3" (111) Si substrates (off-cut 4 along $[01\bar{1}]$) by reactive molecular beam epitaxy (MBE). The native SiO_2 on the silicon wafer was thermally desorbed in the MBE chamber at a substrate temperature of 950 °C. Epitaxial Sc_2O_3 films were grown at a substrate temperature of 400 °C by exposing the clean (111) Si surface to a Sc flux (~2×10^{13} atoms/cm^2·s) in an O_2 background pressure of 5×10^{-8} Torr. The films were capped *in situ* with 15 nm of Al_2O_3 to prevent the Sc_2O_3 films from absorbing moisture. Cross-section and plan-view transmission electron microscopy (TEM) samples were prepared by standard TEM sample preparation techniques with 3 kV Ar ion milling as the final step (Gatan PIPS). High-resolution TEM (HRTEM) was performed using a field-emission TEM (Tecnai F30U) with ultra-twin objective lens (Cs = 0.52 mm), operated at 300 kV.

Despite the large lattice mismatch, x-ray and electron diffraction show single-variant, epitaxial growth with a cube-on-cube orientation relationship that is described by $[111]_{Sc_2O_3} \| [111]_{Si}$ and $(1\bar{1}0)_{Sc_2O_3} \| (1\bar{1}0)_{Si}$. Cross-section HRTEM of the Sc_2O_3/Si interface (Fig. 1) reveals an abrupt interface free of reaction phases, as expected from thermodynamic calculations [16]. Regularly spaced (~1.8 ± 0.1 nm) misfit dislocations with line directions **l** parallel to $[11\bar{2}]_{Si}$ are seen. A Burgers circuit around these dislocations yields an edge component of the Burgers vector of $\mathbf{b}_\perp = 1/4[\bar{1}10]_{Si}$ (inset in Fig. 1). Misfit dislocations are observed in cross-sectional HRTEM along arbitrary <121> directions, whereas no physical dislocations are visible in projections along $[1\bar{1}0]_{Si}$. Therefore, misfit dislocations likely form a hexagonal network with dislocation lines parallel to $[1\bar{2}1]$, $[11\bar{2}]$ and $[\bar{2}11]$. The Burgers vector for this hexagonal network is predicted to be $\mathbf{b} = 1/2[\bar{1}10]_{Si}$ [17]. The network is illustrated in Fig. 2 on a Moiré

pattern. Note that the dislocation spacing projected along $\langle 1\bar{2}1 \rangle$ will be half the spacing between parallel dislocation lines in Fig. 2, and is consistent with the experimentally observed spacing. The image contrast apparently showing $\mathbf{b} = 1/4[\bar{1}10]_{Si}$ dislocations is likely an artifact. A more physically reasonable explanation is that the image contrast is due to two offset arrays of dislocations in an hexagonal array with $\mathbf{b} = 1/2[\bar{1}10]_{Si}$. Image simulations of the observed contrast are currently underway. HRTEM images along $< 1\bar{2}1 >$ also include inclined dislocation segments, as the TEM sample thickness is greater than the dislocation spacing. It appears, however, that the inclined segments do not blur the image contrast between the dislocation cores in Fig. 1. Given their close spacing these dislocations can be considered as an intrinsic part of the interface atomic structure. The dislocations cannot be resolved by diffraction contrast in plan-view TEM.

Plan-view HRTEM images (Figs. 3 and 4) show that the film is comprised of small (10 – 15 nm) domains, separated by planar faults that are frequently parallel to $\{110\}_{Sc_2O_3}$, with a smaller fraction parallel to $\{121\}_{Sc_2O_3}$. Cross-section TEM reveals that the domains are columnar, with boundaries that are slightly curved through the film thickness. We next address the question whether these planar defects are antiphase boundaries (APBs).

The bixbyite structure can be described as a vacancy-ordered fluorite with two oxygen vacancies per fluorite unit cell, causing the bixbyite unit cell parameter to be twice that of fluorite in all three dimensions. When islands of a bixbyite oxide, such as Sc_2O_3, nucleate on Si, they have inherently no unique or energetically preferred arrangement of these ordered oxygen vacancies relative to the Si surface. As island coalesence, antiphase boundaries (APBs) are expected to form between islands that have

their oxygen vacancy sublattices shifted relative to each other. This mechanism of APB formation has been previously observed in other epitaxial systems [18,19]. Possible APBs that leave the cation sublattice unchanged and form due to various arrangements of the oxygen vacancies in the plane of the substrate can be determined by inspection. The displacement vectors across these APBs are of type

$$m/4\left[1\bar{1}0\right]+n/4\left[\bar{1}01\right]+p/4\left[01\bar{1}\right], \quad (1)$$

where *m, n* and *p* are integers between 0 and 3. These displacement vectors are consistent with antiphase domains, which transform into each other by translational operations that are present in the parent (fluorite) structure, but are absent in the domains [20]. The number of distinguishable domain variants (16) can be predicted from group theory [21]. Translational shifts across APBs with a component perpendicular to the beam should be visible in HRTEM, because for thin crystals the symmetry of the image corresponds to the symmetry of the crystal in projection along the electron beam (if the images are aligned and correctly stigmated) [22]. In addition, the magnitude of the shift can be confirmed by comparison of HRTEM image simulations (MacTempas, TotalResolution, Inc.) with experimental images to determine atom column positions across the APB.

Figure 3 shows that the lattice is shifted by $1/4[\bar{1}10]_{Sc_2O_3}$ across the planar fault, consistent with Eq. (1). The inset in Fig. 3 shows an image simulation that matches the experimentally observed contrast and that can be used to identify the projected atom column positions in the experimental image (shown as overlays in Fig. 3). For all images of APBs investigated here image simulations required a non-zero beam tilt to match the experimentally observed contrast away from the boundary. The mosaic structure of the

films (discussed below) makes it difficult to align both sides of the APBs with their zone axes parallel to the beam. The tilt is also likely the origin for the reduction of symmetry in the image. For example, the $\overline{3}$ axes parallel to [111] in bixbyite should project as six-fold axes if imaged along [111]. The simulation shows that due to the tilt, the six-fold symmetry is lost in the image.

Strain contrast due to threading dislocations is observed at APB triple junctions (arrows in Fig. 4). The Burgers circuit shown in Fig. 4, which is mapped onto the Sc sublattice, yields a projected Burgers vector component of $1/12[11\overline{2}]_{Sc_2O_3}$. This Burgers vector component is not a lattice vector and an additional component parallel to the beam is expected. Other circuits yield Burgers vector components of type $n/12[11\overline{2}]_{Sc_2O_3} + m/12[1\overline{2}1]_{Sc_2O_3}$, where *n* and *m* are integers between 0 and 2. Note that the Burgers circuit is insensitive to the oxygen vacancy arrangement and is not influenced by the APBs. Triple junctions formed by APBs described by Eq. (1) should not result in dislocations that produce a Burgers circuit closure failure when mapped onto the Sc sublattice. It is thus likely that these threading dislocations represent geometrically necessary dislocations that account for the misorientation of subgrains with respect to the substrate and/or each other, as expected for a system with a large lattice mismatch [23]. The preferential location of these dislocations at APB triple junctions may be due to two reasons. APB triple junctions represent a defective area of the film, and dislocation may reduce their strain energy if located in these junctions. Secondly, both kinds of extended defects, APBs and threading dislocations, form upon island coalescence and are thus expected to occur in close proximity of each other.

In summary, we have shown Sc_2O_3 can be grown epitaxially on (111) Si. The lattice mismatch between Si and Sc_2O_3 is completely relieved by a hexagonal misfit dislocation network. The films contain a high density of APBs and threading dislocations. APBs are believed to be a general feature of the epitaxy of bixbyite and other fluorite derived structures on Si. It is likely that the applicability of bixbyite films on Si is limited if APBs are to be avoided, for example if they would replicate into an active device area subsequently grown on them.

S. S. thanks Prof. Jim Speck and Prof. Alexei Romanov for discussions. D.O.K. thanks Prof. R. C. Pond for many helpful discussions. This research was supported by the Semiconductor Research Corporation. This work made use of the UCSB MRL central facilities supported by NSF under Awards No. DMR 00-80034 and DMR 0216466. L.F.E. gratefully acknowledges an AMD/SRC fellowship.

REFERENCES

1. *International Technology Roadmap for Semiconductors, 2003 Ed., Front End Processes*, pp. 2, 23–33: http://public.itrs.net/Files/2003ITRS/Home2003.htm (Semiconductor Ind. Assoc., San Jose, 2003).
2. S. Matsubara, N. Shohata, and M. Mikami, Jap. J. Appl. Phys. Part 1 **24,** 10 (1985).
3. D. K. Fork, D. B. Fenner, G. A. N. Connell, J. M. Phillips, and T. H. Geballe, Appl. Phys. Lett. **57,** 1137 (1990).
4. J. W. Seo, J. Fompeyrine, A. Guiller, G. Norga, C. Marchiori, H. Siegwart, and J. P. Locquet, Appl. Phys. Lett. **83,** 5211 (2003).
5. S. Guha, N. A. Bojarczuk, and V. Narayanan, Appl. Phys. Lett. **80,** 766 (2002).
6. L. J. Schowalter and R. W. Fathauer, Crit. Rev. Solid State Mater. Sci. **15,** 367 (1989).
7. M. Morita, H. Fukumoto, T. Imura, Y. Osaka, and M. Ichihara, J. Appl. Phys. **58,** 2407 (1985).
8. H. Fukumoto, T. Imura, and Y. Osaka, Appl. Phys. Lett. **55,** 360 (1989).
9. T. Inoue, Y. Yamamoto, S. Koyama, S. Suzuki, and Y. Ueda, Appl. Phys. Lett. **56,** 1332 (1990).
10. J. Kwo, M. Hong, A. R. Kortan, K. T. Queeney, Y. J. Chabal, J. P. Mannaerts, T. Boone, J. J. Krajewski, A. M. Sergent, and J. M. Rosamilia, Appl. Phys. Lett. **77,** 130 (2000).
11. S. Siskos, C. Fontaine, and A. Munoz-Yague, Appl. Phys. Lett. **44,** 1146 (1984).

12. T. Schleid and G. Meyer, J. Less-Common Met. **149,** 73 (1989).

13. R. D. Shannon, J. Appl. Phys. **73,** 348 (1993).

14. R. Mehandru, B. Luo, J. Kim, F. Ren, B. P. Gila, A. H. Onstine, C. R. Abernathy, S. J. Pearton, D. Gotthold, R. Birkhahn, B. Peres, R. Fitch, J. Gillespie, T. Jenkins, J. Sewell, D. Via, and A. Crespo, Appl. Phys. Lett. **82,** 2530 (2003).

15. H. H. Tippins, J. Phys. Chem. Solids **27,** 1069 (1966).

16. K. J. Hubbard and D. G. Schlom, J. Mater. Res. **11,** 2757 (1996).

17. C. M. Sargent and G. R. Purdy, Philos. Mag. **32,** 27 (1975).

18. D. Hesse, J.Vac. Sci. & Techn. A **5,** 1696 (1987).

19. D. T. Margulies, F. T. Parker, M. L. Rudee, F. E. Spada, J. N. Chapman, P. R. Aitchison, and A. E. Berkowitz, Phys. Rev. Lett. **79,** 5162 (1997).

20. H. Wondratschek and W. Jeitschko, Acta Cryst. A **32,** 664 (1976).

21. C. van Tendeloo and S. Amelinckx, Acta Cryst. A **30,** 431 (1974).

22. J. M. Cowley, in *High-Resolution Transmission Electron Microscopy and Associated Techniques*, edited by P. Buseck, J. Cowley, and L. Eyring (Oxford University Press, New York, 1992), p. 58.

23. V. Srikant, J. S. Speck, and D. R. Clarke, J. Appl. Phys. **82,** 4286 (1997).

FIGURES

Figure 1

Cross-sectional HRTEM micrograph recorded along $[11\bar{2}]_{Si}$. Strain contrast from misfit dislocations is seen periodically along the interface. The inset shows a magnified view of the interface and a Burgers circuit drawn around a dislocation that yields an edge component of the Burgers vector of $\mathbf{b}_{\perp} = 1/4[\bar{1}10]_{Si}$.

Figure 2 (color online)

Schematic of a Moiré pattern formed by two overlapping cubic F-lattices projected along [111] and a hexagonal misfit dislocation network. Filled circles and open circles are bixbyite and diamond lattice points, respectively.

Figure 3 (color online)

Plan-view HRTEM micrograph showing an APB recorded along [111] (the underlying Si was removed by ion-milling). The inset in the upper left corner shows an image simulation with atom positions overlaid. The small (green) circles correspond to Sc and the large (red/white) circles to O in a projection of three adjacent planes along the beam direction. The parameters of the simulation are as follows: sample thickness: 47.5 nm, defocus: 25 nm, tilt: 3 mrad. A small tilt is required in the image simulation to achieve the best match with the experimental image. The overlay across the APB (center) shows a schematic of a projection of one plane and the arrow shows the shift between the two antiphase domains ($1/4[\bar{1}10]_{Sc_2O_3}$). The filled triangles represent Sc-O-vacancy

tetrahedra with lighter shaded triangles showing tetrahedra pointing below the (111) plane and darker shaded triangles tetrahedra pointing above (111).

Figure 4 (color online)

Plan-view HRTEM micrograph of a region of the Sc_2O_3 film from which the underlying Si is removed, showing several APBs (dashed lines) parallel to $\{\bar{1}10\}_{Sc_2O_3}$. Under these imaging conditions bright dots correspond to atom columns. APB triple junctions exhibit strain contrast due to dislocations (block arrows). A Burgers circuit (solid line) is drawn around one dislocation. The inset in the bottom left corner shows the same Burgers circuit transferred to a schematic projection of a fluorite lattice, which shows that the Burgers circuit has a closure failure of $1/12\left[11\bar{2}\right]_{Sc_2O_3}$. A (111) plane of the bixbyite structure is shown for reference.

Figure 1

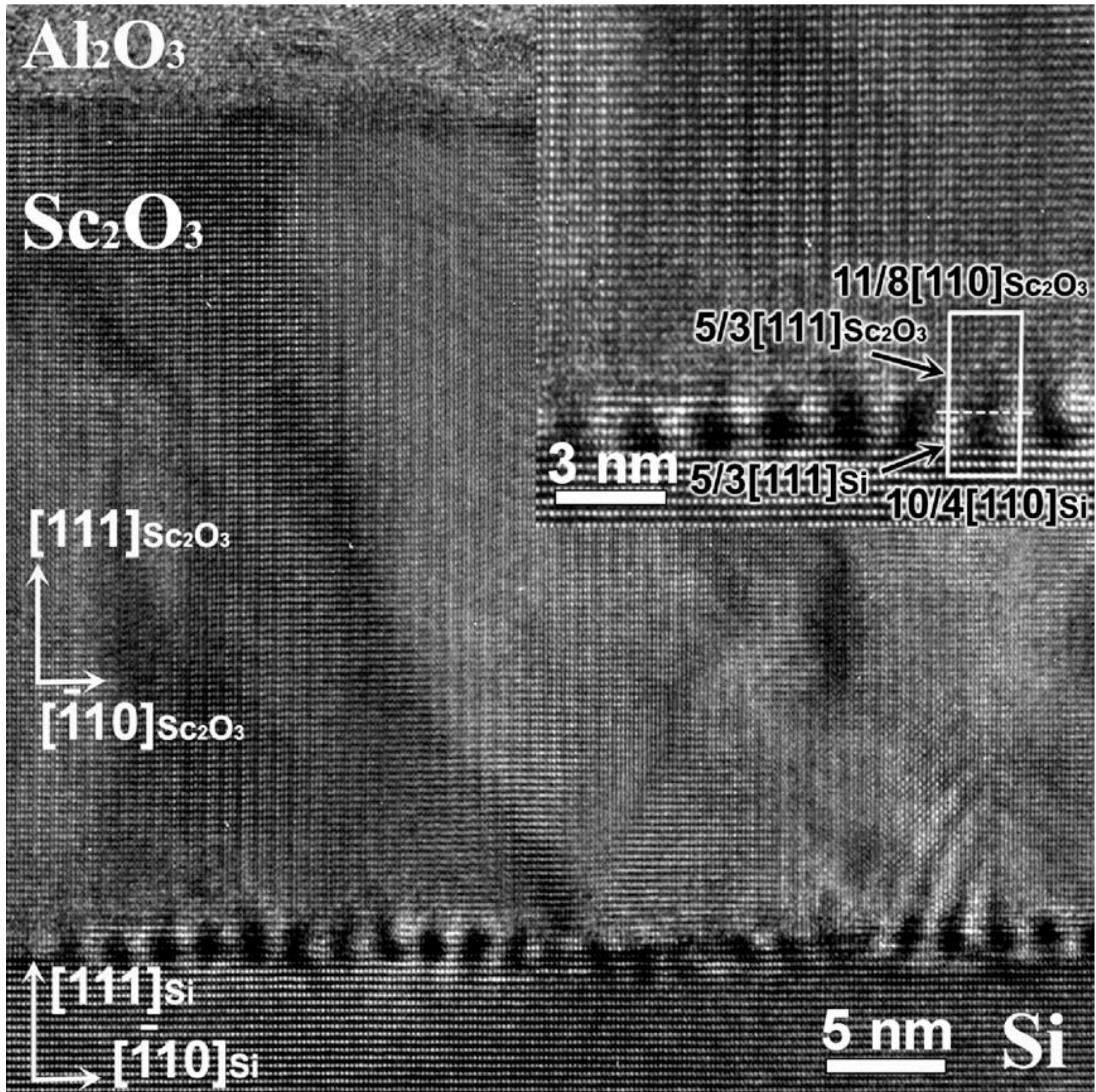

Figure 2

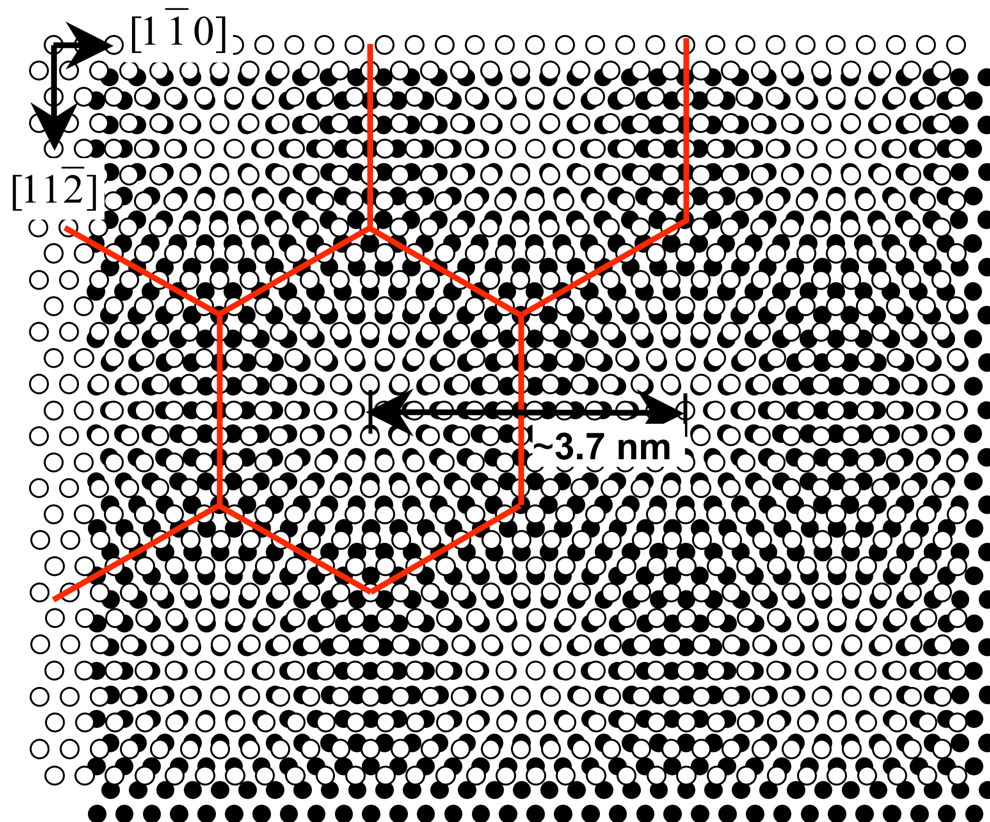

Figure 3

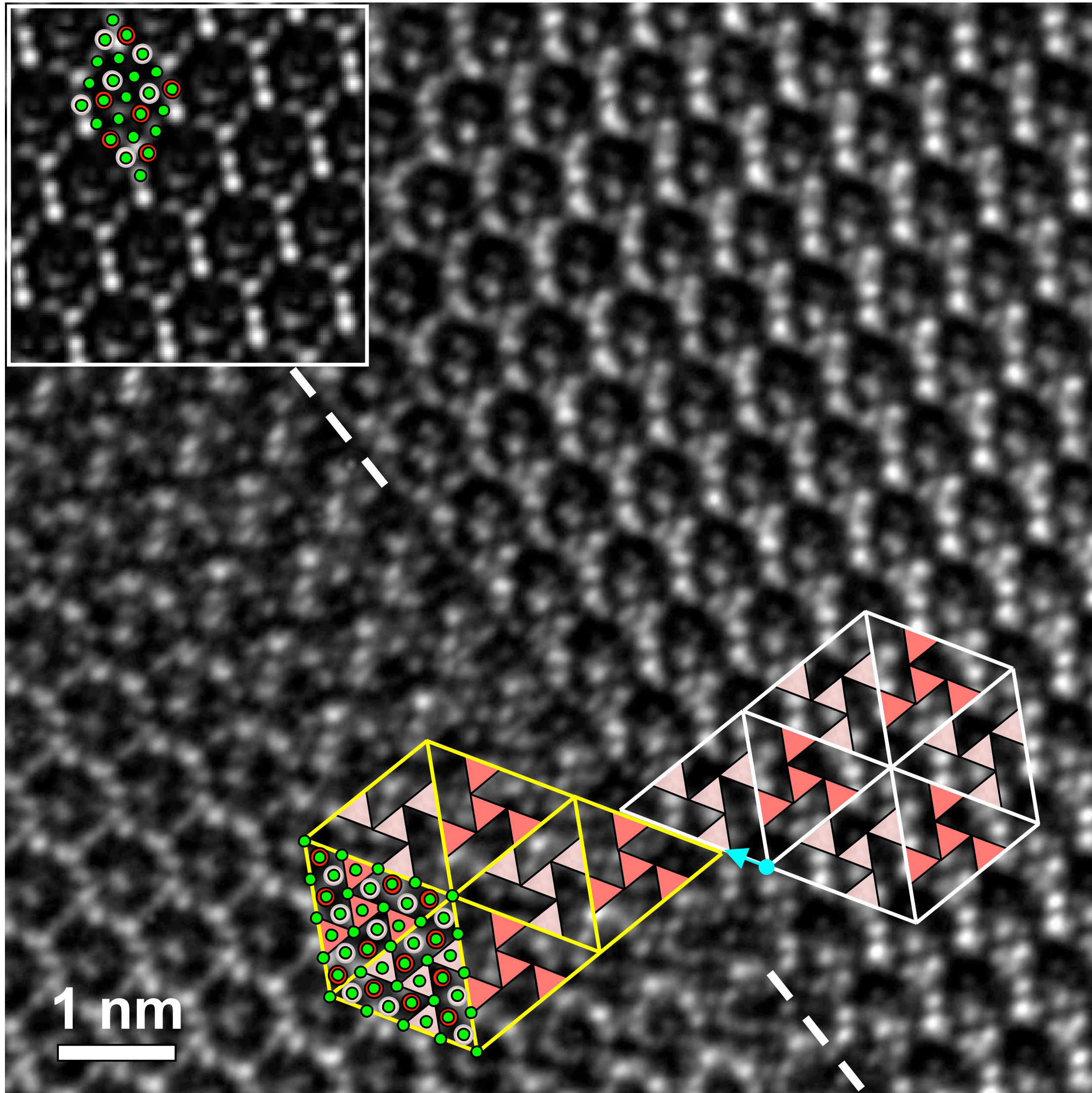

Figure 4